Trans. JSASS Aerospace Tech. Japan
Vol. 14, No. ists30, pp. Pf_89-Pf_96, 2016

# Development and Flight Results of Microsatellite Bus System for RISING-2

By Yuji SAKAMOTO,[1)] Nobuo SUGIMURA,[1)] Kazufumi FUKUDA,[1)] Toshinori KUWAHARA,[1)] Kazuya YOSHIDA,[1)] Junichi KURIHARA,[2)] Tetsuya FUKUHARA[2)] and Yukihiro TAKAHASHI[2)]

[1)] *Department of Aerospace Engineering, Tohoku University, Sendai, Japan*
[2)] *Department of Cosmosciences, Hokkaido University, Sapporo, Japan*

(Received July 31st, 2015)

The RISING-2 microsatellite was launched in May 2014 into a sun-synchronous circular orbit at a height of 628 km. This paper describes the operation results and the flight evaluation of bus system. The satellite was successful in obtaining images of Earth using a high-resolution multi-spectral telescope system with a 5-m spatial resolution in red–green–blue (RGB) observations and 10-m resolution in spectral observations. The weight of the satellite is 43.2 kg, and the shape is almost cubic, with sides 50 cm in length. The satellite has an attitude control system that uses three-axis reaction wheels, which enables a nadir-pointing mode and a target-pointing mode in tracking a specified ground location. The attitude actuators and sensors are magnetic coils, star sensors, gyro sensors, sun sensors, magnetometers, and a global positioning system (GPS) receiver. The satellite attitude could be determined with an error of less than 0.005° from observation images. Using coarse determination methods employing magnetometers, sun sensors, and gyro sensors, the pointing angle error was determined to be 1.9 deg in root mean square (RMS), and the direct distance error was determined to be 21.5 km in RMS.

**Key Words:** Multi-Spectral Telescope, Liquid Crystal Tunable Filter, Attitude Determination, Microsatellite, RISING-2

## 1. Introduction

Microsatellites and nanosatellites have been developed by many universities, educational institutions, and private companies in recent years. Tohoku University has developed and operated two 50-kg microsatellites (SPRITE-SAT and RISING-2) and one 2.6-kg cubesat (RAIKO) since 2006. In addition, two microsatellites (RISESAT, DIWATA) and a new RAIKO-based cubesat are currently being developed.

Our satellite development team considers both of cubesats and 50 kg-class microsatellites to be important to future space engineering. The development of RISING-2 was started in 2009, then the development of cubesat RAIKO was started by inheriting the accumulated knowledge. RAIKO adopted the same communication boards and data handling software developed for RISING-2.[1)] The ground station network for the operation of RAIKO was also used for RISING-2 without any modifications. Cubesats are very effective not only for the rapid space verification of bus system but also for the maturity of ground station network and operation software.

In the last several years, the development of cubesats has grown throughout the world as with microsatellites. A cubesat has a standard size of 10 x 10 x 10 cm and a weight of 1.33 kg. [2)] As extended standards, 3U cubesats with the triple size and weight have become popular in recent years, and 6U cubesats have been suggested as the future standard. The standard for cubesats is becoming the standards for bus units of micro and nanosatellites. Nanosatellites with new shapes, including cubesat bus units and observation instruments with flexible shapes, are now being developed. For example, the AAReST satellite, which combines the seven parts of a 3U cubesat with mirror payloads and a boom structure, functions with a high-precision attitude control and thruster system.[3)] Cubesat kits are utilized not only for cubesats but also for flexible shape nanosatellites and microsatellites. The dimensions and operating procedures of these kits are standardized, and a variety of electrical boards for attitude, communication, and power subsystems are available at low prices.

Although the technologies for cubesats and nanosatellites have been rapidly developed and improved by actual space verifications, microsatellites have still advantageous for Earth observation using high-performance instruments. Because of size, weight, and power restrictions by cubesats, there is a limit to the resolution of the observations that the aperture diameters and focal lengths of the telescopes can provide. [2)] For 50 kg-class microsatellites, Earth observation missions using telescopes are very important and significant functions. In the previous case study about microsatellite telescope system,[4)] a Schmidt-Cassegrain telescope with a 12.7-cm diameter aperture, 1.25-m focal length, and 2.7-kg mass were presumed. These three specifications are similar to those of the telescope of RISING-2. The GRUS satellite by Axelspace Corp. referred to in this paper weights 80 kg and has a 2.5- to 5-m- resolution telescope, although the weight of RISING-2 was 43 kg. High resolution observation by microsatellite telescopes with resolutions of less than 5 m is becoming the goal internationally.

This paper presents a description of the system and initial operation results for the RISING-2 microsatellite, which was

launched on May 24, 2014 by an H-IIA Japanese rocket into a circular orbit with a 628-km altitude. This satellite was successful in capturing ground surface color images with a 5-m spatial resolution and multi-spectral images with a 10-m spatial resolution using the High-Precision Multi-Spectral Telescope System (HPT), and this success exceeded the world's previous best performance in the category of microsatellites weighing less than 50 kilograms. The use of a multi-spectral system using a liquid crystal tunable filter (LCTF) constituted the first such trial ever. This filter permits rapid changes in wavelength from 400 different colors. By establishing observation technologies to compete with previous large and small satellites, micro and nano satellites are expected to become high-performance application satellites or epoch-making constellations.

The attitude determination and control for microsatellites have not been mature, and the analysis by using actual flight data becomes important knowledge for future satellites. In this paper, the performance of attitude determination by conventional typical methods using onboard measurements was evaluated in comparison with the determined attitude from actual observation images. The resolution of observation image by HPT is 659 x 494 pixels, and the ground area in each photo was approximately 3.2 x 2.4 km when the satellite was pointing to nadir. The attitude could be determined from images with an error of 0.005 deg.

The system and mission instruments are described in Section 2. The flight results of the performance verification for the bus subsystems are presented in Section 3. The evaluation results of the coarse attitude determination conducted using magnetometers, sun sensors, and gyro sensors and obtained from an analysis of observation images are presented in Section 4.

## 2. Outline of Satellite System

### 2.1. Bus subsystems

The RISING-2 flight model is shown in Fig. 1, and its internal structure is illustrated in Fig. 2. Table 1 presents key specifications of the system. The satellite is 50 cm on each side and weights 43.2 kg. The orbit is sun synchronous at an altitude of 628 km, and the period is 97.3 minutes. The local time of the descending node is 12 noon.

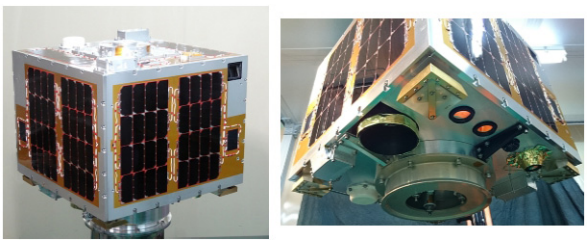

Fig. 1. Illustration of the RISING-2 flight model.

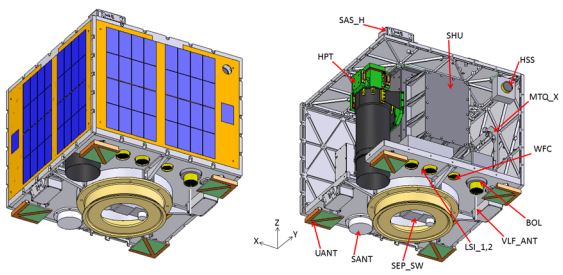


Fig. 2. Illustrations of external and internal structures.

The attitude control system consists of three reaction wheels (RW), three-axis magnetic torquers (MTQ), two star sensors (HSS), a gyro sensor (GYRO), four fine sun sensor units (SASH), coarse sun sensors (SAS) consisting of individual solar cells pasted on side panels, a magnetometer (GAS), and a global positioning system receiver (GPSR), as illustrated in Fig. 3. Except for the GPSR, all of the units in the attitude system were originally developed by university students because the university needed to accumulate the more skills about hardware and the embedded software. The RW and GYRO were replaced by commercial products in the succeeding satellites RISESAT and DIWATA because high-performance units became available from private companies at reasonable prices in these five years.

In the power subsystem, solar cells with 27.1-% efficiency are pasted directly on the side panels. The battery unit is including cells of a nickel-metal hydride (NiMH) battery such as that used in other satellites developed by Tohoku University in the past. The reaction wheels are driven only during observation modes, which duration is 15 minutes in the sunshine phase and 15 minutes in the eclipse phase, because the 47.6-W power generated is not sufficient to maintain constant control of the attitude. The three-axis magnetic torquers can decrease the initial spin motion after the satellite separation, and they are sometimes used to reduce the rotation before the operation mode starts.

The communication speeds are 1200 bit per second (bps) for the command uplink, and a maximum of 100 kilo bps (kbps) for the telemetry downlink, which is 200 kilo symbol per second (ksps) in NRZ-S, Randomize, and Convolution coding. A ground station constructed on the campus of Tohoku University is mainly used for the operation of RISING-2, and the Chiba Institute of Technology is collaborating in cases of emergency. In real operations, a low-speed mode of 25 kbps and a medium-speed mode of 50 kbps are used, and three-piece images with a resolution of 640 x 480 pixels with a 10-bit depth can be downloaded during each observation pass. The output power of transmitter is 100 mW, and two antennas on the top and bottom panel are selected exclusively by a ground command. At the ground station, the ultra-high-frequency (UHF) Yagi antenna with a 10-dB gain and 50-W preamp output is used for the command link, and an S-band receiving antenna with a 2.4-m dish is used for the telemetry link.

Figure 4 shows the relationship of the onboard intelligent units. The satellite central unit (SCU) handles the telemetries and commands, and UHF receiver (URX) and S-band transmitter (STX) are connected. The GAS, SAS, MTQ, and GPSR units are connected to SCU based on concepts associated with the first satellite SPRITE-SAT. The power control unit (PCU), the attitude control unit (ACU) and the science handling unit (SHU) communicate with the SCU via an RS422 interface. The stable functioning of these four units are ensured by industrial grade field-programmable gate arrays (FPGA) and microcontrollers. For maximum reliability,

Table 1. List of system specifications.

| | |
|---|---|
| **Mass, Size, Life** | |
| mass | 43.2 kg |
| size | 50 x 50 x 50 cm |
| design life | > 1 year |
| **Orbit** | |
| type | Sun Synchronous Orbit |
| altitude | 628 km |
| orbit period | 97.3 min / rev |
| localtime | 12:00 (noon) at descending node |
| **Attitude determination and control** | |
| type | 3-axis active control using reaction wheels |
| sensors | star sensors, gyro sensors, sun sensors, magnetometers |
| actuators | reaction wheels, magnetic coils |
| **Power** | |
| generation | 47.6 W (GaAs, 27.1% efficiency) |
| consumption | 31.2 W (obs. mode, max.) |
| | 11.9 W (typical) |
| | 5.1 W (power saving), 3.3W (emergency) |
| battery | NiMH, 3.7AH, 10.8V (= 40WH) |
| **Communication** | |
| command | UHF-band, 1200bps |
| telemetry | S-band, 0.1W out, 100kbps max. |

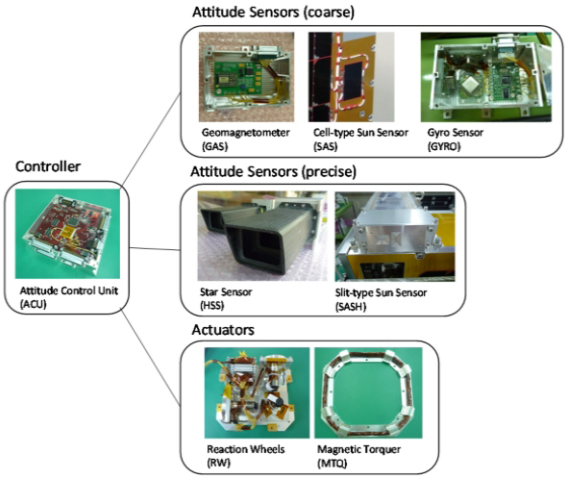


Fig. 3. Units used in attitude determination and control subsystem.

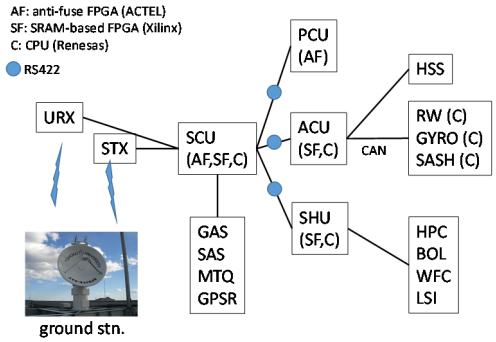


Fig. 4. Data communication of onboard units.

anti-fuse FPGAs (Actel RTSX32SU) are used in the SCU and PCU. SRAM-based FPGAs (Xilinx Virtex2, Virtex4) and microcontrollers (Renesus SH7145F, H8/36057) are also used for large-area logic circuits and attitude calculation programs.

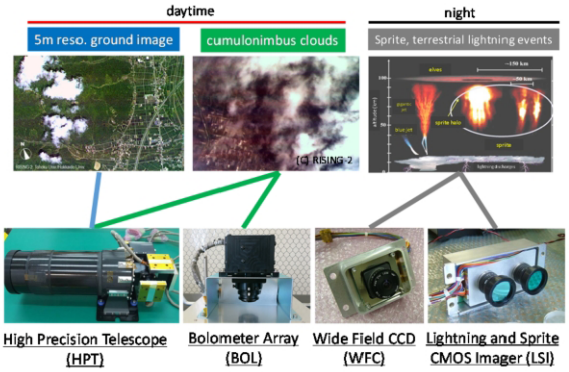


Fig. 5. Scientific missions and onboard instruments.

### 2.2. Mission subsystems

Figure 5 shows the onboard instruments used for scientific missions. The primary mission of the satellite is to obtain 5 m-resolution images of the ground surface using a multi-spectral high precision telescope (HPT). The satellite has other image sensors: a wide-field sensor (WFC) using charge-coupled device (CCD) for wide-area ground surface images, a bolometer array (BOL) for sensing the temperature distribution of cumulonimbus clouds, and lightning and sprite imager (LSI) for sensing lightning and sprite phenomena.

The HPT is a Cassegrain-type optical telescope with a 10-cm caliber (F10) and 1-m focal length. There are two modes of observation, a 400-650 nm visible color image mode (HPC-RGB, using three CCD sensors) and a 650-1050 nm multi-spectral image mode (HPC-M using one CCD sensor with a LTCF). The wavelength of the HPC-M can be varied within the range of 39-259 msec from 400 colors.

The BOL is the mid-infrared sensor, which has a field view of 48.6 x 36.5 degrees, a wavelength range of 8-14 μm, and a spatial resolution of approximately 1 km. The distribution of cloud heights can be determined from captured images of cumulonimbus clouds. The resolution is 640 x 480 pixels, with a 16-bit pixel depth.

The LSI consists of two complementary metal oxide semiconductor (CMOS) imagers, which are an LSI-W with a range of 744-826 nm and an LSI-N with 762nm. The field of view is 27.8 x 27.8 degrees, the pixel field is 512 x 512 pixels, and a spatial resolution of 600 m, 1.2 km, or 2.4 km can be selected.

The WFC can be used for Earth observations during either the daytime or night-time. The field of view is 134 x 180 degrees.

### 2.3. Pre-flight evaluation for bus subsystems

The development of RISING-2 began in 2009, and the flight model was completed in approximately 18 months, which permitted implementation of an effective development process and rapid environmental tests.

The attitude sensors, actuators, and computer for RISING-2 were developed by university students and staff members. Detail of the development have been published in previous papers.[5-7] The development and upgrading of the ground evaluation simulator are important research topics.[8] The attitude motion and estimated sensor outputs are calculated by the ground computer, and the dummy outputs are supplied to the flight hardware. By this hardware-in-the-loop simulation

(HILS) process, the validity of the onboard software can be evaluated correctly. The outputs of the flight actuators are also returned to the simulation software, and the attitude motion is updated. This simulator equipment is also used to evaluate the power charge/discharge system.

The same ground transmitter and receiver are used in electrical system tests, and the commands and telemetries are communicated, using connected radio-frequency (RF) cables, between the satellite flight model and the ground support equipment (GSE).

The design and evaluation of the structure subsystem have matured on the bases of experience with three 50 kg-class microsatellites.[9] However, the structure weight is now exceeding 20% of the total mass, and this must be decreased to permit the addition of more payload resources. In the RISING-2 development, four-time vibration tests were carried out using the Mechanical Test Model (MTM), which consists of an evaluation structure and dummy masses, as well as a one-time test using the Evaluation Model (EM), and a one-time test using the Flight Model (FM). The total number of tests could be decreased by comparison to the results for the first satellite, SPRITE-SAT.[10]

## 3. Operation Results

RISING-2 was successfully launched from Tanegashima on May 24, 2014 at 12:05:14pm (JST) by the H-IIA rocket #24. The ground station at Tohoku University communicates with the satellite in an average of two passes during the daytime and two passes during the night-time. The duration of one pass is approximately 12 minutes.

### 3.1. Mission instruments

The observations by the WFC, HPC-RGB, and HPC-M can be carried out by established procedures. The images obtained by the BOL require the post processing by methods that have not been established. The LSI can be used only on the eclipse side, and practical observations have not been achieved by the instability of star sensors.

After the third day of operation, trial observations with the WFC were started. By adjusting the exposure time and the CCD gain values, stable procedures for both the daytime and the night were established. Even on the night side, the shape of the Earth and the lights of urban areas could be distinguished as shown in Fig. 6. In a recent photo, most of the Japanese islands could be clearly observed on a sunny day.

After two weeks of operation, trial observations with the HPT were begun. To achieve the appropriate focus, the mirrors had to be heated to approximately 20 degC. After calibrating of the attitude determination and control algorithms, the first reasonable photo was successfully obtained on July 2, 2014 with a 5-m resolution as shown in Fig. 7. At present, several photographs have been acquired as shown in Fig. 8.

Observations with the HPC-M are more difficult than with the HPC-RGB because a longer exposure time is required to obtain reasonably brighten images to overcome the decreased light by the LCTF. The ground location in which the satellite is pointed must not be changed during the exposure time.

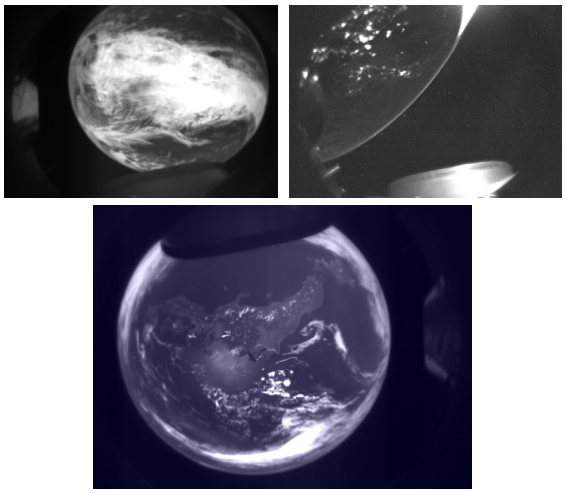

Fig. 6. WFC observation images: At the upper left is the first daytime image obtained on May 31, 2014, and at the upper right is the first nighttime image obtained on June 7, 2014. The lower image is an image of the Japanese islands obtained on a sunny day, May 2, 2015.


Fig. 7. HPC-RGB observation image: The first reasonable ground image obtained with 5-m resolution, taken on July 2, 2014. The location is N37.106767 and E138.886075 in Niigata, Japan.

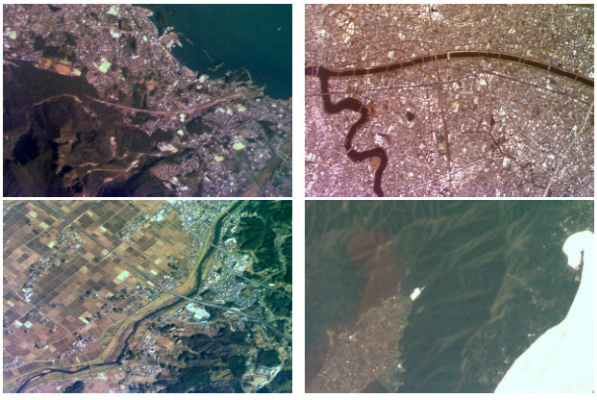

Fig. 8. Examples of HPC-RGB observation image.

After the procedure for the HPC-RGB was established, the first reasonable images were obtained on August 20, 2014. By increasing the attitude pointing stability, observations with 1/60-sec exposure times could be established when the attitude stability was less than 0.0374 deg/s.

### 3.2. Bus subsystems

**1) Communication:** The input signal level of the onboard UHF receiver is - 126 dBm without signals and increases to the range of - 109 to - 100 dBm in command operations. The link margin is between +10 and +19 dB.

**2) Temperature:** At the summer solstice on June 21, 2014,

the temperature of internal structure was 9.9 degC and the temperature of battery was 13.1 degC during daytime operations. These temperatures increased to 12.6 degC and 14.7 degC, respectively, during night-time operations. The estimation temperatures for the battery were 14.7 degC in the summer, 19.8 degC in the spring/winter, and 24.3 degC in the winter. The actual temperature of the battery was lower by 4.8 degC, and the temperature is expected to remain within the safe range in future operations.

**3) Battery voltage:** The final date of charging before launch was April 4, 2014, and the launch date was May 24, 2014. Although a little natural discharging was expected, the initial power condition was normal. The battery charging and discharging system has been working well since the launch. The 0.5-C charging is automatically stopped at an equivalent voltage of 13.13 V, which is the converted voltage assuming a temperature of 25 degC and no charging current. Using this method, the battery capacity can be evaluated correctly, independent of the effects of the temperature and current. The low-voltage mode is initiated when the discharging voltage is lower than eigher 9.9 V or 9.0 V, as selected by ground command. In this mode, all the onboard units, except for the PCU, URX, and SCU, are powered off automatically, and the satellite operates at its lowest consumption power level of 3.3W until the start of the sunshine phase. In actual operation, this mode occurs safely several times when the attitude and scientific units are not turned off after the completion of the observation mode.

**4) SCU functions:** For the telemetry and command operations, only the SRAM-based FPGA is necessary, the CPU programs are optional. Using CPU programs, the recording and playback of housekeeping data and the stored command function (time-designated commands) can be used.

**5) Attitude control by magnetic torquers:** De-spin control by the torquers was started on the third day of operation. Based on the gyro measurement, the initial spin speed was estimated to be 1.48 deg/s after the separation. Single-axis control was carried out for 60 minutes for each axis, and the decrease in the spin rate was confirmed. If the plus/minus of the torquer axis is mistaken, the current can be reversed by ground command. On the fifth day during the daytime, the spin rate was decreased to 0.23 deg/s. On the first satellite SPRITE-SAT, the solar cells pasted on the panels generated a magnetic moment, and the satellite attitude was seriously affected. The current direction (clockwise or not) of the RISING-2 was managed by parallel cells, so that the total magnetic moment was reduced to zero. It was confirmed the spin rate could not be changed naturally after the torquer control was stopped.

**6) Attitude control by reaction wheels:** In the first week operation, a trial of the automatic nadir pointing control was started. In this trial, the ACU software measured the GAS, SAS, and sending commands to the reaction wheels. The correct status telemetries, including the target attitude, current attitude, and error angles, were confirmed. The correct axis direction of each wheel was then confirmed by rotating the each wheel at +2000 rpm and -2000 rpm. Using the automatic sequence of the ACU software, the error angle was decreased to less than 10 degrees, and a WFC photograph with the entire Earth at the center could be successfully obtained. During the second-week trial, a target location with an east longitude and a north latitude was uploaded by commands, and target pointing control was attempted. In this mode, the target attitude is continuously updated, and the pointing axis is locked onto the target location. However, this mode was not achieved successfully because the magnetic field model in the onboard program was assumed based on a simple single-order magnet in which the angle error of the magnetic vector is at most 35 degrees according to numerical simulation results. The magnetic field can be calculated using the latest International Geomagnetic Reference Field (IGRF). It was difficult to integrate a more precise model because of the low program memory and slow computational speed. In the successor satellite, a five-order IGRF model was integrated by devising the required calculation procedures. The precision was improved less than 1 deg in root mean squares (RMS). The sun sensors were affected by albedo lights, and the result of attitude determination changed frequently. Each sensor consisted of a general solar power cell without any filters, and a total of six cells were pasted on six panels. The solar angle was estimated by simple cosine conversion from measurement currents. Functions of sensitivity adjustment and polynomial conversion were integrated in successor satellites. Because of the insufficient attitude determination, the appropriate calculation of automatic control commands could not be established in practical level, and so a new attitude determination method was required to achieve the required control. To address this difficulty, a new control program was prepared in the ground operation computer. Although the measurement interval is every 1 second, several new algorithms were tested efficiently without the onboard program update. The ground program calculates the attitude using the GAS, SAS, GYRO, and GPS measurements, and commands to change the wheel speed are uploaded every second. When the target error is less than specific acceptance level, an observation trigger command is automatically sent to the satellite. Using this new method, the target pointing control was successfully established.

**7) Star Sensors:** Trials using the star sensors were begun during the first week. The star sensors were able to function during the night time, but had difficulty functioning during the daytime. Bright lights existed near the edge lines of hood structure, and the onboard algorithm could not remove these white lines. In addition, white spots gradually became more prominent as a result of the effect of radiation. At present, the onboard program does not function correctly even during the night time. However, the satellite can download the images obtained by the star sensors. By accumulating many star images, a new image processing algorithm could be established in which the tolerance for white spots could be increased. An update function for the onboard program was not prepared for this satellite, but an improved star sensor will be used in future satellites.

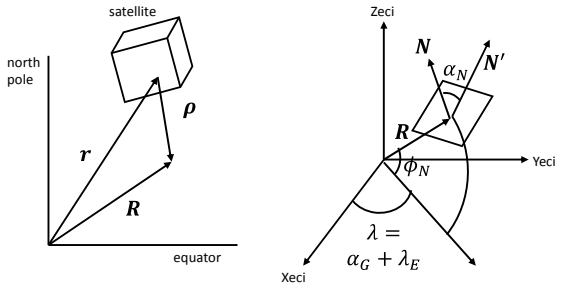


Fig. 9. Attitude determination by observation images.

## 4. Attitude Determination Using Magnetometers, Sun Sensors, Gyro Sensors, and Observation Images

The resolution of the star sensors is 0.06 deg/pixel, and the error of the determined attitude is less than 0.1 degrees. Coarse determination methods are still useful because the fine determination methods that use the star sensor data have some limitations including the fact that they cannot be used when solar light or albedo light enters. When the mission does not require high-precision determination or when its field of view is wide, the coarse determination methods will be sufficient.

### 4.1. Theory

#### (1) Orbit determination by triad method

The triad method is an easy and traditionally convenient attitude determination method.[11] The attitude can be determined from the measurements of the magnetic vector and sun vector in the body-fixed frame without other prior or subsequent measurements.

The magnetic vector $\overline{\boldsymbol{B}}_{\boldsymbol{I}}$ and sun vector $\overline{\boldsymbol{S}}_{\boldsymbol{I}}$ in the Earth-centered inertia coordinate frame (ECI) can be solved from the mathematical models. The onboard measurements are $\boldsymbol{B}_m$ and $\boldsymbol{S}_m$ in the body-fixed frame. The transformation matrix $A_{I,e}$ from the ECI to the body-fixed frame is as follows:

$$A_{I,e} = M_m (M_I)^T \tag{1}$$

where

$$\boldsymbol{M} = \begin{bmatrix} \boldsymbol{q_0} & \boldsymbol{r_0} & \boldsymbol{s_0} \\ \boldsymbol{q_1} & \boldsymbol{r_1} & \boldsymbol{s_1} \\ \boldsymbol{q_2} & \boldsymbol{r_2} & \boldsymbol{s_2} \end{bmatrix} \tag{2}$$

$$\boldsymbol{q} = \boldsymbol{B}/|\boldsymbol{B}|,\ \boldsymbol{v} = \boldsymbol{S}/|\boldsymbol{S}| \tag{3}$$

$$\boldsymbol{r} = (\boldsymbol{u} \times \boldsymbol{v})/|\boldsymbol{u} \times \boldsymbol{v}|,\ \boldsymbol{s} = \boldsymbol{q} \times \boldsymbol{r} \tag{4}$$

#### (2) Averaging of measurements

Averaged measurements are used for the attitude determination because the $\boldsymbol{B}_m$, $\boldsymbol{S}_m$, and the gyro measurements $\boldsymbol{\omega}_m$ include measurement noise. For example, the new $2n$+1 data (duration of $2\Delta t$) are used as follows:

$$\overline{\boldsymbol{B}}_{m,t-\Delta t} = \frac{1}{2n+1}\sum_{i=1}^{2n+1} \boldsymbol{B}_{mi} \quad \overline{\boldsymbol{S}}_{m,t-\Delta t} = \frac{1}{2n+1}\sum_{i=1}^{2n+1} \boldsymbol{S}_{mi} \tag{5}$$

$$\overline{\boldsymbol{\omega}}_m = \frac{1}{n}\sum_{i=1}^{n} \boldsymbol{\omega}_{mi} \tag{6}$$

where $\overline{\boldsymbol{B}}_{m,t-\Delta t}$ and $\overline{\boldsymbol{S}}_{m,t-\Delta t}$ are the average values at time $t - \Delta t$, and the $\overline{\boldsymbol{B}}_m$ and $\overline{\boldsymbol{S}}_m$ at the most recent time $t$ are estimated using the angular velocity $\overline{\boldsymbol{\omega}}_m$.

Table 2. List of observation image locations.

| Image ID | Time (JST = UTC + 9h) YY/MM/DD | Image Location north lat. (deg) $\phi_N$ | east lon. (deg) $\lambda_E$ | azimuth (deg) $\alpha_N$ | Satellite Position north lat. (deg) | east lon. (deg) | alt. (km) |
|---|---|---|---|---|---|---|---|
| 1 | 14/09/11 12:53:41 | 37.607 | 126.565 | 46.9 | 34.984 | 126.736 | 634.514 |
| 2 | 14/12/02 12:09:44 | 35.557 | 139.242 | 55.6 | 35.806 | 137.627 | 630.501 |
| 3 | 14/12/09 12:49:46 | 32.766 | 130.363 | 54.8 | 32.335 | 126.897 | 631.271 |
| 4 | 14/12/17 12:09:08 | 35.736 | 139.392 | 55.8 | 38.670 | 138.361 | 633.133 |
| 5 | 14/12/27 12:08:25 | 38.253 | 140.347 | 56.5 | 39.951 | 138.806 | 634.132 |
| 6 | 15/01/05 11:48:44 | 36.121 | 139.907 | 49.0 | 38.492 | 143.361 | 633.726 |
| 7 | 15/01/05 11:49:22 | 36.222 | 140.079 | 58.7 | 36.178 | 142.695 | 633.258 |
| 8 | 15/04/28 12:22:50 | 35.325 | 135.647 | 38.2 | 35.295 | 135.702 | 632.407 |
| 9 | 15/05/08 12:18:55 | 35.433 | 137.242 | 46.7 | 35.347 | 137.301 | 631.414 |

Fig. 10. Example of observation images (ID = 1, ID = 3).

Table 3. Error angles of measurement vectors (ID = 1).

| Sensor | Axis | meas. (A) $\boldsymbol{S}_m$ | revised meas. (A) $\overline{\boldsymbol{S}}_m$ | determined by image (A) $\overline{\boldsymbol{S}}_e$ | angle error (deg) $\varepsilon_s$ |
|---|---|---|---|---|---|
| Sun | e1 | 0.209 | 0.115 | 0.165 | 4.8 |
| | e2 | 0.061 | 0.073 | 0.004 | |
| | e3 | -0.990 | -0.924 | -0.993 | |

| Sensor | Axis | meas. (gauss) $\boldsymbol{B}_m$ | revised meas. (gauss) $\overline{\boldsymbol{B}}_m$ | determined by image (gauss) $\overline{\boldsymbol{B}}_e$ | angle error (deg) $\varepsilon_b$ |
|---|---|---|---|---|---|
| Magnet | e1 | -0.046 | -0.067 | -0.051 | 3.3 |
| | e2 | 0.093 | 0.071 | 0.084 | |
| | e3 | 0.324 | 0.365 | 0.347 | |

Table 4. Evaluation of measurement errors and attitude determination.

| Image ID | Error Angles Sun (deg) $\varepsilon_s$ | Magnet (deg) $\varepsilon_b$ | Roll (deg) | Pitch (deg) | e3 (deg) | Pointed Location Error North (km) | East (km) | Direct (km) |
|---|---|---|---|---|---|---|---|---|
| 1 | 4.8 | 3.3 | -1.7 | -0.1 | 1.7 | 8.9 | 32.1 | 33.3 |
| 2 | 0.8 | 1.3 | 0.2 | -3.2 | 3.2 | 2.2 | -35.1 | 35.2 |
| 3 | 5.4 | 4.1 | -1.3 | -0.8 | 1.5 | 4.0 | 14.2 | 14.7 |
| 4 | 3.8 | 3.9 | -1.1 | -1.6 | 1.9 | 2.4 | -1.0 | 2.6 |
| 5 | 1.3 | 0.3 | -2.0 | -0.1 | 2.0 | 9.1 | 29.9 | 31.2 |
| 6 | 5.5 | 1.6 | -1.4 | -0.5 | 1.5 | 3.4 | 13.7 | 14.1 |
| 7 | 3.5 | 2.7 | -0.4 | -1.0 | 1.1 | 13.3 | -5.3 | 14.3 |
| 8 | 1.3 | 0.5 | -0.9 | -1.0 | 1.3 | -3.7 | 6.7 | 7.7 |
| 9 | 3.8 | 3.8 | -1.5 | -1.7 | 2.3 | -10.5 | 7.1 | 12.6 |
| RMS | 3.8 | 2.8 | 1.3 | 1.4 | 1.9 | 7.4 | 20.2 | 21.5 |

Using the rotation unit vector $\overline{\boldsymbol{\omega}}_m/|\overline{\boldsymbol{\omega}}_m|$ and the rotation scalar angle $n|\overline{\boldsymbol{\omega}}_m|$, the quaternion $\boldsymbol{q}_{\Delta t}$ and the cosine direction matrix $A_{\Delta t}$ can be calculated. Then, $\overline{\boldsymbol{B}}_{m,t-\Delta t}$ and $\overline{\boldsymbol{S}}_{m,t-\Delta t}$ can be converted to $\overline{\boldsymbol{B}}_{m,t}$ and $\overline{\boldsymbol{S}}_{m,t}$ as follows:

$$\overline{\boldsymbol{B}}_{m,t} = A_{\Delta t}\overline{\boldsymbol{B}}_{m,t-\Delta t} \quad \overline{\boldsymbol{S}}_{m,t} = A_{\Delta t}\overline{\boldsymbol{S}}_{m,t-\Delta t} \tag{7}$$

#### (3) Attitude determination from observation images

The satellite attitude can be determined from the images obtained by the HPT. The location coordinates, east longitude $\lambda_E$, north latitude $\phi_N$, and the azimuth $\alpha_N$ of upper direction, can be determined from each image using web-based mapping

software. At the time of observation, the satellite position is converted from GPS data. The satellite has a GPS receiver, and the real time position can be obtained every second.

The satellite position vector is defined by $\boldsymbol{r}$, the position vector of observed ground location is defined by $\boldsymbol{R}$, and the relative vector $\boldsymbol{\rho}$ is solved as shown in Fig. 9. The upper direction of the photo is defined by $\boldsymbol{N'}$, and the three axes $\boldsymbol{e}_1, \boldsymbol{e}_2,$ and $\boldsymbol{e}_3$ of the body-fixed frame can be solved as follows:

$$\boldsymbol{\rho} = \boldsymbol{R} - \boldsymbol{r} \tag{8}$$

$$\boldsymbol{e}_3 = \frac{\boldsymbol{\rho}}{|\boldsymbol{\rho}|} \quad \boldsymbol{e}_2 = -\frac{\boldsymbol{\rho}\times\boldsymbol{N'}}{|\boldsymbol{\rho}\times\boldsymbol{N'}|} \quad \boldsymbol{e}_1 = \boldsymbol{e}_2 \times \boldsymbol{e}_3 \tag{9}$$

The transformation matrix from the ECI to the body-fixed frame is as follows:

$$\boldsymbol{e}_i = [e_{i1} \quad e_{i2} \quad e_{i3}]^T \tag{10}$$

$$A_e = \begin{bmatrix} e_{11} & e_{12} & e_{13} \\ e_{21} & e_{22} & e_{23} \\ e_{31} & e_{32} & e_{33} \end{bmatrix} \tag{11}$$

This matrix can be converted to the quaternion $\boldsymbol{q}_e$.

Defining the longitude of Greenwich at the time of observation as $\alpha_G$, $\boldsymbol{N'}$ can be solved as follows:

$$\lambda = \alpha_G + \lambda_E \tag{12}$$

$$\boldsymbol{N'} = \left(C^1_{-\alpha_N} C^2_{-\phi_N} C^3_{\lambda}\right)^T \begin{bmatrix} 0 \\ 0 \\ 1 \end{bmatrix} \tag{13}$$

where

$$C^1_\theta = \begin{bmatrix} 1 & 0 & 0 \\ 0 & \cos\theta & \sin\theta \\ 0 & -\sin\theta & \cos\theta \end{bmatrix} \quad C^2_\theta = \begin{bmatrix} \cos\theta & 0 & -\sin\theta \\ 0 & 1 & 0 \\ \sin\theta & 0 & \cos\theta \end{bmatrix}$$

$$C^3_\theta = \begin{bmatrix} \cos\theta & \sin\theta & 0 \\ -\sin\theta & \cos\theta & 0 \\ 0 & 0 & 1 \end{bmatrix} \tag{14}$$

With respect to the sun vectors, the estimation vector in the ECI from the mathematical model is defined by $\overline{\boldsymbol{S}}_{\boldsymbol{I}}$, the vector in the body-fixed frame determined from the image is defined by $\hat{S}_e$, and the real measurements in the body-fixed frame are defined by $S_m$ as follows:

$$\widehat{\boldsymbol{S}}_{\boldsymbol{e}} = A_e \overline{\boldsymbol{S}}_{\boldsymbol{I}} \quad \widehat{\boldsymbol{S}}_{\boldsymbol{m}} = M_{\boldsymbol{st}} \boldsymbol{S}_{\boldsymbol{m}} \tag{15}$$

where $M_{\boldsymbol{st}}$ is transformation matrix to optimal values that minimizes the errors of $\hat{S}_e$ and $\widehat{\boldsymbol{S}}_{\boldsymbol{m}}$. $M_{\boldsymbol{st}}$ is solved as follows:

$$M_{se} = [\widehat{\boldsymbol{S}}_{m1} \quad \cdots \quad \widehat{\boldsymbol{S}}_{mn}] \quad M_{\boldsymbol{sm}} = [\boldsymbol{S}_{\boldsymbol{m1}} \quad \cdots \quad \boldsymbol{S}_{\boldsymbol{mn}}] \tag{16}$$

$$M_{se} = M_{st} M_{sm} \tag{17}$$

$$M_{st} = (M_{se} M_{sm}^T)\left(M_{sm} M_{sm}^T\right)^{-1} \tag{18}$$

### 4.2 Evaluation of onboard sensors and attitude determination using images

As a case study, the onboard measurements and the determined attitude were evaluated using the images listed in Table 2. Example photos are shown in Fig. 10.

The calibration matrix $M_{st}$ can be solved by calculating the matrix $M_{se}$ of the estimated sun vector and the matrix $M_{sm}$ of the onboard measurements vector. The calibration matrix $M_{bt}$ for magnetic sensor can be solved in the same manner. The calculated calibration matrices are as follows:

$$M_{st} = \begin{bmatrix} 0.711 & -0.189 & 0.000 \\ -0.071 & 0.793 & -0.016 \\ -0.124 & -0.058 & 0.902 \end{bmatrix} \tag{19}$$

$$M_{bt} = \begin{bmatrix} 0.898 & -0.202 & -0.043 \\ 0.014 & 0.971 & -0.029 \\ -0.068 & -0.007 & 1.107 \end{bmatrix} \tag{20}$$

where $M_{st}$ and $M_{bt}$ can calibrate the sensitivity offsets of each axis and the alignment offset errors. For the sun sensor, the averaged albedo effects can be removed.

The observation vectors in ID = 1 are listed in Table 3. The angle errors of $\widehat{\boldsymbol{S}}_{\boldsymbol{m}}$ and $\widehat{\boldsymbol{S}}_{\boldsymbol{e}}$, and the angle errors of $\widehat{\boldsymbol{B}}_{\boldsymbol{m}}$ and $\widehat{\boldsymbol{B}}_{\boldsymbol{e}}$ were calculated. The sun vector error $\varepsilon_s$ was 4.8 deg, and the magnetic vector error $\varepsilon_b$ was 3.3 deg.

Using the same procedure, the angle errors were solved for ID = 2 to 9 images. Then, using the calibrated $\widehat{\boldsymbol{S}}_{\boldsymbol{m}}$ and $\widehat{\boldsymbol{B}}_{\boldsymbol{m}}$, the attitude $\boldsymbol{q}_m$ was determined using the triad method. The offset roll and pitch angles with respect to the attitude $\boldsymbol{q}_e$ determined from the image were evaluated, and the distance errors on the target ground surface were also calculated. The results are summarized in Table 4. The rotation order of the roll, pitch, and yaw is e1, e2, and e3, that is, the yaw angle does not affect the target location error.

The RMS errors were 3.8 deg for the sun vector, 2.8 deg for the magnetic vector, 1.3 deg for the roll angle, 1.4 deg for the pitch angle, and 1.9 degrees for the body-fixed e3 axis. The target location RMS errors were 7.4 km in the north-south direction, 20.2 km in the east-west direction, and 21.5 km in direct distance. Using the image-based attitude determination, the onboard sensor errors and the pointing accuracy could be evaluated quantitatively.

In this analysis, the observations of the sun sensor and the magnetic sensor were affected by the bias offset errors of the gyro sensors. By averaging the measurements from the latest 8-second data, the observations were rotated by the gyro measurements. For this reason, the errors for both sensors were larger than others for image IDs 1, 3, 4, and 9.

## 5. Conclusions

The specifications of microsatellite RISING-2 and its initial operation results are described in this paper. The radio communication, onboard temperature, and battery conditions have remained safe and stable from launch to the present time. Stable observations of the WFC, HPC-RGB, and HPC-M were also established using target pointing control. New star sensors are being developed from the accumulated star images obtained by RISING-2. The onboard measurement errors and the pointing accuracy were evaluated quantitatively using real observation images. The error angles of the sun vector and magnetic vector were 3.8 and 2.8 deg in RMS, respectively. The pointing accuracy was 1.9 deg (RMS) in angle error and 21.5 km (RMS) in distance.

## References


1) Sakamoto, Y., Tanabe, Y., Yagisawa, H., Sugimura, N., Yoshida, K., Nishio, M., Nakajo, T. and Akiyama, H.: Operation Results of Cubesat RAIKO Released from International Space Station, *Trans. JSASS, Aerospace Tech. Japan*, **12**, ists29( 2014), pp.Tf_7-Tf_12.
2) Selva, D. and Krejci, D.: A Survey and Assessment of the Capabilities of Cubesats for Earth Observation, *Acta Astronautica*, **74**(2012), pp.50-68.
3) Underwood, C., Pellegrino, S., Lappas, V. J., Bridges, C. P. and

Baker, J.: Using CubeSat/Micro-Satellite Technology to Demonstrate the Autonomous Assembly of a Reconfigurable Space Telescope (AAReST), *Acta Astronautica*, **114**(2015), pp.112-122.
4) Roberto, R. D., Nascetti, A., Paolozzi, A. and Paris, C.: Optical Payload for High-Resolution Earth Imaging Suitable for Microsatellites, *IEEE 15th International Conference on Environment and Electrical Engineering (EEEIC)*, 2015.
5) Kuwahara, T., Battazo, S., Tomioka, Y., Fukuda, K., Sakamoto, Y. and Yoshida, K.: System Integration of a Star Sensor for the Small Earth Observation Satellite RISING-2, *Trans. JSASS*, *Aerospace Tech. Japan*, **10,** ists28(2012), pp.Td_1-Td_6.
6) Fukuda, K., Sugimura, N., Sakamoto, Y., Kuwahara, T., Yoshida, K. and Takahashi, Y.: The Evaluation Tests of the Attitude Control System of the 50-kg Micro Satellite RISING-2, *Trans. JSASS*, *Aerospace Tech. Japan*, **10,** ists28(2012), pp.Td_11-Td_16.
7) Sugimura, N., Fukuda, K., Tomioka, Y., Fukuyama, M., Sakamoto, Y., Kuwahara, T., Fukuhara, T., Yoshida, K. and Takahashi Y.: Ground Test of Attitude Control System for Micro Satellite RISING-2, *2012 IEEE/SICE International Symposium on System Integration*, 2012, pp.301-306.
8) Tomioka, Y., Fukuda, K., Sugimura, N., Sakamoto, Y., Kuwahara, T. and Yoshida, K.: Establishment of the Ground Testing Environment for Verification and Integration of Micro-satellite, *Trans. JSASS*, *Aerospace Tech, Japan*, **12,** ists29(2014), pp.Tf_33-Tf_38.
9) Tomioka, Y., Yoshida, K., Sakamoto, Y., Kuwahara, T., Fukuda, K. and Sugimura, N.: Lessons Learned on Structural Design of 50kg Micro-Satellites Based on Three Real-Life Micro-Satellite Projects, *2012 IEEE/SICE International Symposium on System Integration*, 2012, pp.319-324.
10) Yoshida, K., Takahashi, Y., Sakamoto, Y., Ujiie, E., Takiuchi, K., Nakazato, Y., Sawakami, T., Sakanoi, T., Kasaba, Y., Kondo, S., Yamashida, K., Ueda, S., Takashima, T., Nakazawa, K., Mitani, T., Enoto, T., Sato, M., Inan, U., Linscott, I., Bruhn, F. and Masumoto, Y.: SPRITE-SAT: a Micro Satellite for Scientific Observation of Transient Luminous Events and Terrestrial Gamma-Ray Flashes, *Trans. JSASS*, *Aerospace Tech. Japan*, **8,** ists27(2010), pp.Tm_7-Tm_12.
11) Wertz, J. R. (Editor): *Spacecraft Attitude Determination and Control*, Astrophysics and Space Science Library, Springer, 1978.